J. Fluid Mech. (1976), *vol.* 78, *part* 1, *pp.* 49–63
Printed in Great Britain

Unsteady evolution of a horizontal jet in a stratified fluid

By R. PEYRET

Laboratoire de Mécanique Théorique associé au C.N.R.S., Université Pierre et Marie Curie, Place Jussieu, 75005 Paris, France

(Received 5 May 1975 and in revised form 4 May 1976)

The unsteady laminar flow due to the penetration of a horizontal jet of constant density into a stratified fluid is considered. A numerical solution of the Navier–Stokes equations under the Boussinesq approximation is obtained by means of an implicit finite-difference method. Results for different values of the Reynolds and internal Froude numbers are given and discussed.

1. Introduction

Recent advances in numerical methods applied to fluid mechanics now permit the use of such methods to study the fundamental character of flows which are too complicated to be solved by analytical methods. The problem considered here belongs to this class. More precisely, this paper is concerned with the unsteady evolution of a laminar horizontal jet in a stratified fluid initially at rest. This problem, which has various applications (e.g. to the behaviour of a fluid discharge into a stratified reservoir or lake), is considered here in the case where the internal Froude number is sufficiently small to induce noticeable 'upstream influence'.

Theoretical or experimental studies of jets and plumes in a stratified medium are rather numerous: results and references can be found in the recent book by Turner (1973) or else in the survey article by Gebhart (1973). Among the most recent work on the subject, we mention that of Tenner & Gebhart (1971), List (1971) and Maxworthy (1972). The last two references consider the case of a horizontal jet, which differs fundamentally from the vertical case generally studied.

Very little numerical work based on the solution of the Navier–Stokes equations has been done on this subject or on related problems. Except for the studies by Wessel (1969) and by Young & Hirt (1972), who considered the special case of the evolution in time of a given volume of homogeneous fluid embedded in a stratified environment, the only work is due to Trent & Welty (1973), who were, in fact, concerned only with the steady vertical case. Even unsteady jet flows of a homogeneous fluid have been studied very little by means of numerical solution of the Navier–Stokes equations: to our knowledge, this problem has only been considered by Fromm (1967) and, recently, by Grant (1974).

The physical problem is described in § 2 and the corresponding mathematical problem is defined in § 3. In § 4, the finite-difference method is described and § 5 is devoted to a discussion of the numerical results.

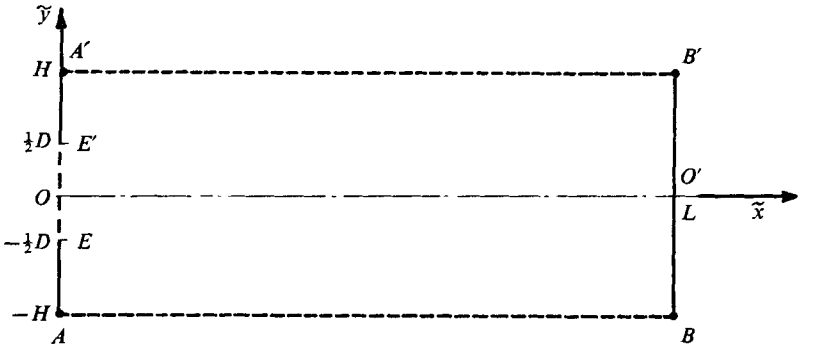

FIGURE 1. Geometrical configuration.

2. The physical problem

We consider the unsteady evolution of a laminar horizontal plane jet in a stratified fluid. A rectangular basin $ABB'A'$ (figure 1) of length $AB = A'B' = L$ and height $AA' = BB' = 2H$ is filled with a viscous incompressible fluid, initially at rest and linearly stratified in temperature:

$$T(\tilde{y}) \equiv T_s(\tilde{y}) = (2H)^{-1}(T_2 - T_1)\,\tilde{y} + \tfrac{1}{2}(T_2 + T_1). \tag{2.1}$$

Thus $T = T_1$ at the bottom AB ($\tilde{y} = -H$) and $T = T_2$ at the top $A'B'$ ($\tilde{y} = H$). We assume $T_2 > T_1$, so that the stratification is statically stable.

The density ρ is related to the temperature T by the equation of state

$$\rho = \rho_0[1 - \beta(T - T_0)], \tag{2.2}$$

where β is the volume coefficient of thermal expansion; the reference quantities ρ_0 and T_0 are defined here by

$$\rho_0 = \tfrac{1}{2}(\rho_1 + \rho_2), \quad T_0 = \tfrac{1}{2}(T_1 + T_2), \tag{2.3}$$

where ρ_1 and ρ_2 are respectively the values of the density at the bottom and the top.

From (2.1) and (2.2), the initial density distribution ρ_s of the fluid inside the tank is

$$\rho(\tilde{y}) \equiv \rho_s(\tilde{y}) = \rho_0[1 - (\beta/2H)\,(T_2 - T_1)\,\tilde{y}], \tag{2.4}$$

and the pressure p is hydrostatic, i.e.

$$p(\tilde{y}) \equiv p_s(\tilde{y}) = -g\rho_0[\tilde{y} - (\beta/4H)\,(T_2 - T_1)\,\tilde{y}^2] + \text{constant}, \tag{2.5}$$

where g is the gravitational acceleration.

Now, from the time $t = 0$, fluid is progressively injected, with a parabolic velocity profile, into the tank from a vertical slot EE' of height D located on AA' symmetrically with respect to the horizontal axis $O\tilde{x}$ (i.e. EE' corresponds to $\tilde{x} = 0$, $|\tilde{y}| \leqslant \frac{1}{2}D$). The physical properties of the injected fluid are the same as those of the surrounding fluid at rest, but its temperature is constant and equal to T_0. Therefore its density is also constant, and equal to ρ_0, the local

density at $\tilde{y} = 0$ of the fluid initially at rest. Simultaneously, fluid leaves the basin vertically at AB and at $A'B'$ with opposite vertical velocities partly determined by the condition of conservation of volume flux.

The above choice of geometrical configuration was suggested by the experimental work of Maxworthy (1972). However, in Maxworthy's experiments the jet was injected into a tank with a free surface. The correct numerical treatment of a free surface is very complicated and, although the description of the motion of the fluid near the free surface would be interesting, it was not our purpose here and we have chosen, in a first treatment of the problem, to locate the fixed top at a (hopefully) sufficiently large distance from the slot ($OA'/OE' = 7{\cdot}125$) and to simulate the rising free surface by imposing a vertical exit velocity. For simplicity the boundary condition at the bottom has been chosen to yield a symmetrical solution and computation can therefore be restricted to the half-domain $OABO'$. Consideration of a more realistic boundary condition (zero velocity at the bottom) would destroy the symmetry and, in order to maintain the same accuracy, would necessitate twice as many discretization points. Note that, in the present calculations, the magnitude of the exit velocity is equal to 0·0344 times the maximum value U_0 of the velocity at the entry.

In other ways also we have chosen to depart significantly from the experimental conditions (as regards, for example, the size of the tank and the magnitude of the diffusion) in order to be able to minimize the effects of the inherent numerical errors due to discretization and consequently to be confident about the accuracy of the results. Hence comparison with the experimental results of Maxworthy (1972) can be at best qualitative; this comparison will show that the main features of the flow observed experimentally are reproduced by the numerical solution.

3. The equations of motion

The problem is studied by numerical solution of the Navier–Stokes equations under the Boussinesq approximation:

$$\rho_0(\partial \mathbf{U}/\partial \tilde{t} + \mathbf{U}.\tilde{\nabla}\mathbf{U}) + \tilde{\nabla} p = \mu \tilde{\nabla}^2 \mathbf{U} - g\rho \mathbf{j}, \tag{3.1}$$

$$C_p \rho_0(\partial T/\partial \tilde{t} + \mathbf{U}.\tilde{\nabla} T) = K \tilde{\nabla}^2 T, \tag{3.2}$$

$$\tilde{\nabla}.\mathbf{U} = 0, \tag{3.3}$$

where $\mathbf{U}$ is the velocity, μ and K are respectively the coefficients of viscosity and of thermal conductivity, C_p is the specific heat at constant pressure, $\mathbf{j}$ is a unit vector in the vertical direction and $\tilde{\nabla} = (\partial/\partial\tilde{x}, \partial/\partial\tilde{y})$.

We now introduce the perturbation quantities $\tilde{\pi}$, $\tilde{\theta}$ and $\tilde{\tau}$ with respect to the corresponding values p_s, T_s and ρ_s for the fluid at rest:

$$p = p_s + \tilde{\pi}, \quad T = T_s + \tilde{\theta}, \quad \rho = \rho_s + \tilde{\tau}. \tag{3.4}$$

Finally, the non-dimensional variables

$$\left.\begin{aligned} x = \tilde{x}/2D, \quad y = \tilde{y}/2D, \quad t = (U_0/2D)\tilde{t}, \quad \tau = \tilde{\tau}/\rho_0, \\ \mathbf{V} = (u, v) = \mathbf{U}/U_0, \quad \pi = \tilde{\pi}/\rho_0 U_0^2, \quad \theta = \tilde{\theta}/(T_2 - T_1) \end{aligned}\right\} \tag{3.5}$$

are considered, so that (3.1)–(3.3) become

$$\frac{\partial \mathbf{V}}{\partial t} + \mathbf{V}.\nabla\mathbf{V} + \nabla\pi = \frac{1}{R}\nabla^2\mathbf{V} + \frac{\eta}{F^2}\theta\mathbf{j}, \tag{3.6}$$

$$\frac{\partial \theta}{\partial t} + \mathbf{V}.\nabla\theta + \frac{1}{\eta}\mathbf{V}.\mathbf{j} = \frac{1}{RP}\nabla^2\theta, \tag{3.7}$$

$$\nabla.\mathbf{V} = 0, \tag{3.8}$$

where τ has been eliminated by using the equation of state (2.2). In (3.6)–(3.8) several non-dimensional parameters appear:

$$\left.\begin{aligned} R = 2D\rho_0 U_0/\mu, \quad P = \mu C_p/K, \quad \eta = H/D, \\ F^{-2} = g\beta\frac{T_2 - T_1}{2H}\left(\frac{2D}{U_0}\right)^2 = g\frac{\rho_1 - \rho_2}{2H\rho_0}\left(\frac{2D}{U_0}\right)^2, \end{aligned}\right\} \tag{3.9}$$

where R is the Reynolds number, P the Prandtl number, η a shape parameter and F the internal Froude number. Note that the buoyancy force in (3.6) is characterized by the parameter ηF^{-2}.

The initial conditions at $t = 0$ are

$$u(x, y, 0) = v(x, y, 0) = \theta(x, y, 0) = 0, \tag{3.10}$$

therefore $\pi(x, y, -0) = 0$. The boundary conditions, as described in § 2, are now specified.

(*a*) Along AA', $x = 0$,

$$u(0, y, t) = \begin{cases} \phi(t)(1 - 16y^2) & \text{if } |y| \leqslant \frac{1}{4}, \\ 0 & \text{if } \frac{1}{4} < |y| < \frac{1}{2}\eta, \end{cases} \tag{3.11a}$$

$$v(0, y, t) = 0 \qquad \text{if } |y| < \tfrac{1}{2}\eta, \tag{3.11b}$$

$$\theta(0, y, t) = \begin{cases} -y/\eta & \text{if } |y| \leqslant \frac{1}{4}, \\ 0 & \text{if } \frac{1}{4} < |y| < \frac{1}{2}\eta. \end{cases} \tag{3.11c}$$

(*b*) Along BB', $x = x_1 = L/(2D)$, $|y| < \frac{1}{2}\eta$,

$$u(x_1, y, t) = v(x_1, y, t) = \theta(x_1, y, t) = 0. \tag{3.12}$$

(*c*) Along AB ($y = -\frac{1}{2}\eta$) and $A'B'$ ($y = \frac{1}{2}\eta$), $0 < x < x_1$,

$$\left.\begin{aligned} u(x, \pm\tfrac{1}{2}\eta, t) &= 0, \\ v(x, \pm\tfrac{1}{2}\eta, t) &= \pm\phi(t)\mathscr{V}(x), \\ \theta(x, \pm\tfrac{1}{2}\eta, t) &= 0. \end{aligned}\right\} \tag{3.13}$$

The function $\phi(t)$ in (3.11) allows for a smooth increase in the velocity of the injected fluid from zero at $t = 0$ to its final steady value at $t = t_0$; we have chosen a polynomial satisfying $\phi(0) = \phi'(0) = \phi'(t_0) = 0$ and $\phi(t_0) = 1$,

viz. $$\phi(t) = \begin{cases} t^2[t^2 - 2(t_0 + t_0^{-3})t + t_0(t_0 + 2t_0^{-3})] & \text{if } t \leqslant t_0, \\ 1 & \text{if } t > t_0. \end{cases} \tag{3.14}$$

It has been confirmed numerically that, as expected, the flow at subsequent times is not sensitive to the particular form chosen for the function $\phi(t)$.

The function $\mathscr{V}(x)$, which characterizes the vertical exit velocity, is assumed to be a constant A except near the corners of the tank; more precisely,

$$\mathscr{V}(x) = \left\{\begin{array}{ll} Ax & \text{if } 0 \leqslant x < x_0, \\ Ax_0 & \text{if } x_0 \leqslant x < x_1 - x_0, \\ A(x_1 - x) & \text{if } x_1 - x_0 < x \leqslant x_1, \end{array}\right\} \tag{3.15}$$

with $x_0 = \frac{3}{160}x_1$ and the constant A, which is determined by the conservation of volume flux, given by $A = 1/6(x_1 - x_0)$.

With these initial and boundary conditions the solution of (3.6)–(3.8) possesses the following symmetry properties:

$$\left.\begin{array}{ll} u(x, -y, t) = u(x, y, t), & v(x, -y, t) = -v(x, y, t), \\ \pi(x, -y, t) = \pi(x, y, t), & \theta(x, -y, t) = -\theta(x, y, t). \end{array}\right\} \tag{3.16}$$

The range of the physical parameters which will be considered in the numerical computation makes it reasonable to assume that the flow remains laminar and symmetrical. For the values of the Reynolds number used here ($R = 10$ and 100) the large values of F^{-2} considered ($F^{-2} = 32$ and 64) ensure the validity of this assumption. In the case $F^{-2} = 0$, it is possible that a real flow does not remain symmetrical for $R = 100$,† but the case $F^{-2} = 0$ is considered here only for comparison, the emphasis being on the stratified case.

Thus the numerical solution is computed in the lower half-domain $y < 0$ with the following conditions on the axis $y = 0$:

$$\partial u(x, 0, t)/\partial y = v(x, 0, t) = \theta(x, 0, t) = 0. \tag{3.17}$$

4. The numerical method

The finite-difference scheme used for solving the problem is an implicit scheme of the Crank–Nicholson type. The spatial derivatives are approximated with second-order-accurate centred differences except for the convective derivatives in the θ equation, which are discretized with fourth-order-accurate differences. The last choice was made in order to minimize the magnitude of the truncation error associated with these convective terms compared with the diffusion term, which has the coefficient $1/RP$, which can be small. The grid is the one used in the MAC method (Harlow & Welch 1965). The computational domain is divided into square cells (i, j) of side h; the pressure π is defined at the centre of each cell, the horizontal and vertical velocity components u and v are respectively defined at the mid-points of the vertical and horizontal edges of the cell, and finally the temperature θ is defined at the corners (see figure 6 in the appendix).

† However, note that experimental (Beavers & Wilson 1970) and numerical (Grant 1974) studies have shown that jets emitted in an infinite environment remain symmetrical for higher Reynolds numbers.

In order to simplify the notation, we introduce the symbols u_h, v_h, θ_h and π_h to represent the values of the unknowns, i.e.

$$u_h \equiv u^{n+1}_{i+\frac{1}{2},j}, \quad v_h \equiv v^{n+1}_{i,j+\frac{1}{2}}, \quad \theta_h \equiv \theta^{n+1}_{i+\frac{1}{2},j+\frac{1}{2}}, \quad \pi_h \equiv \pi^{n+\frac{1}{2}}_{i,j},$$

where n is the index of time, so that $t = nk$, where k is the time step. The finite-difference equations are written in the symbolic form

$$\mathscr{L}_u(u_h, v_h, \pi_h) = 0, \quad \mathscr{L}_v(u_h, v_h, \pi_h, \theta_h) = 0, \tag{4.1a,b}$$

$$\mathscr{L}_\theta(u_h, v_h, \theta_h) = 0, \quad \mathscr{D}(u_h, v_h) = 0. \tag{4.1c,d}$$

Equations (4.1 a, b) correspond to the momentum equations, (4.1 c) is the temperature equation and (4.1 d) is the incompressibility condition. Their forms are given in the appendix.

The accuracy of the scheme is $O(k^2, h^2)$ and, owing to its implicit character, it is expected to be unconditionally stable. The symmetry conditions at $y = 0$ are imposed by introducing extra rows of points outside the computational domain. The spatial derivatives of u, v and θ near the boundaries are approximated by non-centred [for u and v in (4.1 a, b)] and centred [for θ in (4.1 c)] differences with second-order accuracy.

The solution of the nonlinear algebraic system determining the unknowns u_h, v_h, θ_h and π_h is obtained by the iterative procedure used by Fortin (1972), Begis (1972) and also by Childress & Peyret (1976); a related method was proposed by Chorin (1968). This iterative procedure, characterized by the index ν, is defined by

$$u_h^{\nu+1} - u_h^\nu + \kappa \mathscr{L}_u(u_h^\nu, v_h^\nu, \pi_h^\nu) = 0, \tag{4.2a}$$

$$v_h^{\nu+1} - v_h^\nu + \kappa \mathscr{L}_v(u_h^{\nu+1}, v_h^\nu, \pi_h^\nu, \theta_h^\nu) = 0, \tag{4.2b}$$

$$\theta_h^{\nu+1} - \theta_h^\nu + \chi \mathscr{L}_\theta(u_h^{\nu+1}, v_h^{\nu+1}, \theta_h^\nu) = 0, \tag{4.2c}$$

$$\pi_h^{\nu+1} - \pi_h^\nu + \lambda \mathscr{D}(u_h^{\nu+1}, v_h^{\nu+1}) = 0, \tag{4.2d}$$

and is initiated with the values of u_h, v_h, θ_h and π_h at the previous time level.

The values chosen for the constant parameters κ, χ and λ must ensure convergence. Necessary conditions for convergence can be obtained by a study of the stability of the scheme (4.2) considered as an approximation of a 'time-dependent' system (ν being the index of 'time'). The system (4.2) is simplified by neglecting convective and gravitational terms. Then, by imposing the condition that the spectral radius of the associated matrix of amplification should not exceed one, we get the conditions

$$\left.\begin{gathered} \kappa > 0, \quad \chi > 0, \quad \lambda > 0, \\ 2\frac{\kappa}{h^2}\left(\frac{1}{R} + \frac{h^2}{4k} + \lambda\right) \leqslant 1, \quad 2\frac{\chi}{h^2}\left(\frac{1}{RP} + \frac{h^2}{4k}\right) \leqslant 1. \end{gathered}\right\} \tag{4.3}$$

These conditions were found to be sufficient for effective computations.

Note the following particular points concerning the numerical procedure.

(i) In order to improve the convergence, the iterative procedure described above was modified by using in each of (4.2 a–d) the values of the corresponding unknowns at iteration $\nu + 1$ as soon as they were computed (the Gauss–Seidel technique).

(ii) The optimal values of the parameters κ, χ and λ were determined by numerical tests. For given values of κ and χ, the best convergence is obtained with a value of λ close to the maximum allowed by (4.3).

(iii) Convergence of the iterative procedure is assumed to be obtained when

$$\max\{|\mathscr{L}_u|, |\mathscr{L}_v|, |\mathscr{L}_\theta|, |\mathscr{D}|\} < \epsilon.$$

By taking account of the magnitude $O(k^2, h^2)$ of the truncation error corresponding to the values of k and h ($k = \frac{1}{64}$ and $h = \frac{1}{16}$), the value of ϵ was chosen between 3×10^{-3} and 4×10^{-3} depending on the case considered and on the phase in time (initial or succeeding phase). Generally, the maximum value of the residues is given by the momentum equation (either u_h or v_h); then the divergence equation is satisfied to within less than 10^{-3} and the θ_h equation to within less than $1{\cdot}2 \times 10^{-5}$. The number of iterations necessary to achieve convergence varies with the values of flow parameters (the Reynolds and Froude numbers). In the initial phase ($t \leqslant t_0 = 0{\cdot}25$) this number lies between 50 and 150, and when $t > 0{\cdot}25$ it varies between 10 and 50. The computations were stopped at $t = 1{\cdot}50$.

5. Discussion of numerical results

All the calculations were done for $x_1 = L/(2D) = 5$, $\eta = H/D = 3{\cdot}5625$, $t_0 = 0{\cdot}25$, $P = 10$, $h = \frac{1}{16}$, $k = \frac{1}{64}$ and $\chi = \kappa$. Two values of the Reynolds number were considered: $R = 10$ and $R = 100$. For each, computations were performed with three different values of the internal Froude number: $F^{-2} = 0$, 32 and 64. We used $\kappa = 0{\cdot}195 \times 10^{-2}$ and $\lambda = 0{\cdot}875$ for $R = 10$ and $\kappa = 0{\cdot}293 \times 10^{-2}$ and $\lambda = 0{\cdot}59$ for $R = 100$. Some results have already been presented (Peyret 1974).

The profiles of horizontal velocity u at several vertical sections (x = constant) in the tank and at various times are shown in figure 2. These profiles correspond to the lower half $ABO'O$ of the domain and must be completed by symmetry. The form of the u profiles clearly shows the effect of stratification. The fluid injected at $x = 0$ pushes ahead of it the ambient fluid, which remains, to some extent, channelled by the effect of the buoyancy force, which tends to prevent downward motion (upward in the upper region $y > 0$). Hence the perturbations created by the penetration of the jet are felt at very large distances ahead of it. This explains the velocity profiles observed at these distances (e.g. $x \gtrsim 1{\cdot}20$ at $t = 1{\cdot}50$), which have large maxima on the axis $y = 0$ (the evolution of the velocity on the axis is shown in figure 3). The phenomenon of 'upstream influence' is characteristic of slow stratified flows for which F^{-2} is sufficiently large. Several theoretical as well as experimental studies (see, for example, Martin & Long 1968; Pao 1968; Graebel 1969) have exhibited such behaviour in the case of the slow motion of a body in a stratified fluid.

The velocity profiles (figure 2) are quite similar to those obtained experimentally by Maxworthy (1972). The characteristic wavy shape of the profiles corresponds to the presence of eddies and reverse flows. Although it is known in the case of perturbations created by the motion of a body (Martin & Long 1968; Pao 1968) that the wavy shape is not due to end effects, it is likely that the influence of the end BB' is not entirely negligible in our results (any more than

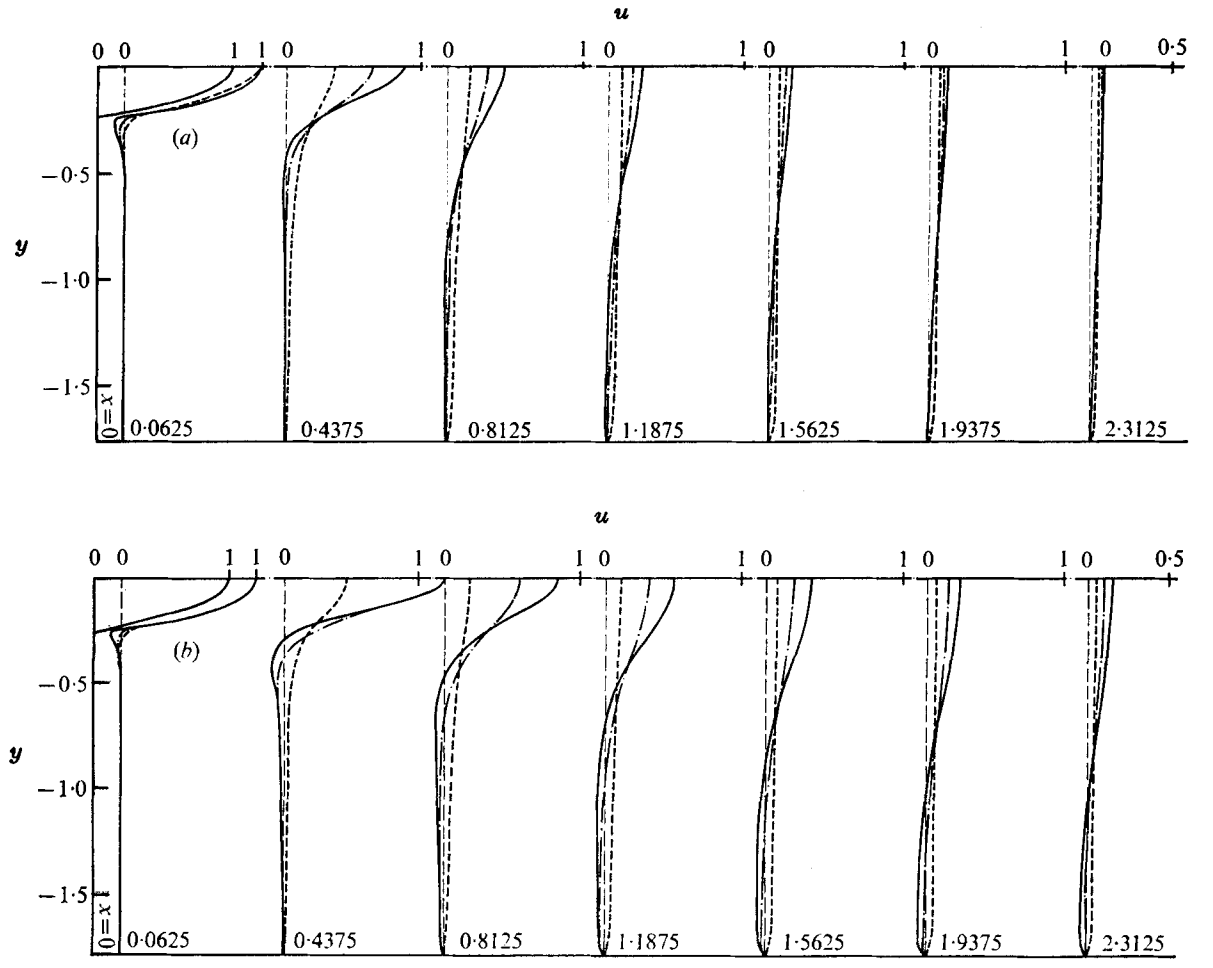

FIGURES 2(*a*, *b*). For legend see facing page.

in the experimental results of Maxworthy). The end effect becomes more important as time increases and ultimately plays a dominant role in the development of backflow.

One of the interesting features of the flow is the presence of eddies. For example, in the case $R = 100$, $F^{-2} = 64$ a primary eddy appears near the entrance at $t = 0{\cdot}30$ approximately. (We recall that the entry velocity has reached its steady value of one at $t = t_0 = 0{\cdot}25$.) This eddy is convected by the flow while being diffused. Then, around $t = 0{\cdot}85$, a second eddy appears, still near the entrance. In order to illustrate the flow pattern, the streamlines $\psi =$ constant at $t = 0{\cdot}75$ and $t = 1{\cdot}50$ are given in figures 4(*a*) and (*b*), which show the lower half of the field. For comparison, we have drawn in figure 4(*c*) the streamlines at $t = 1{\cdot}50$ in the case $R = 100$, $F^{-2} = 0$, i.e. without buoyancy effects.

Note that at $t = 1{\cdot}50$ (when the computations were stopped) the flow is

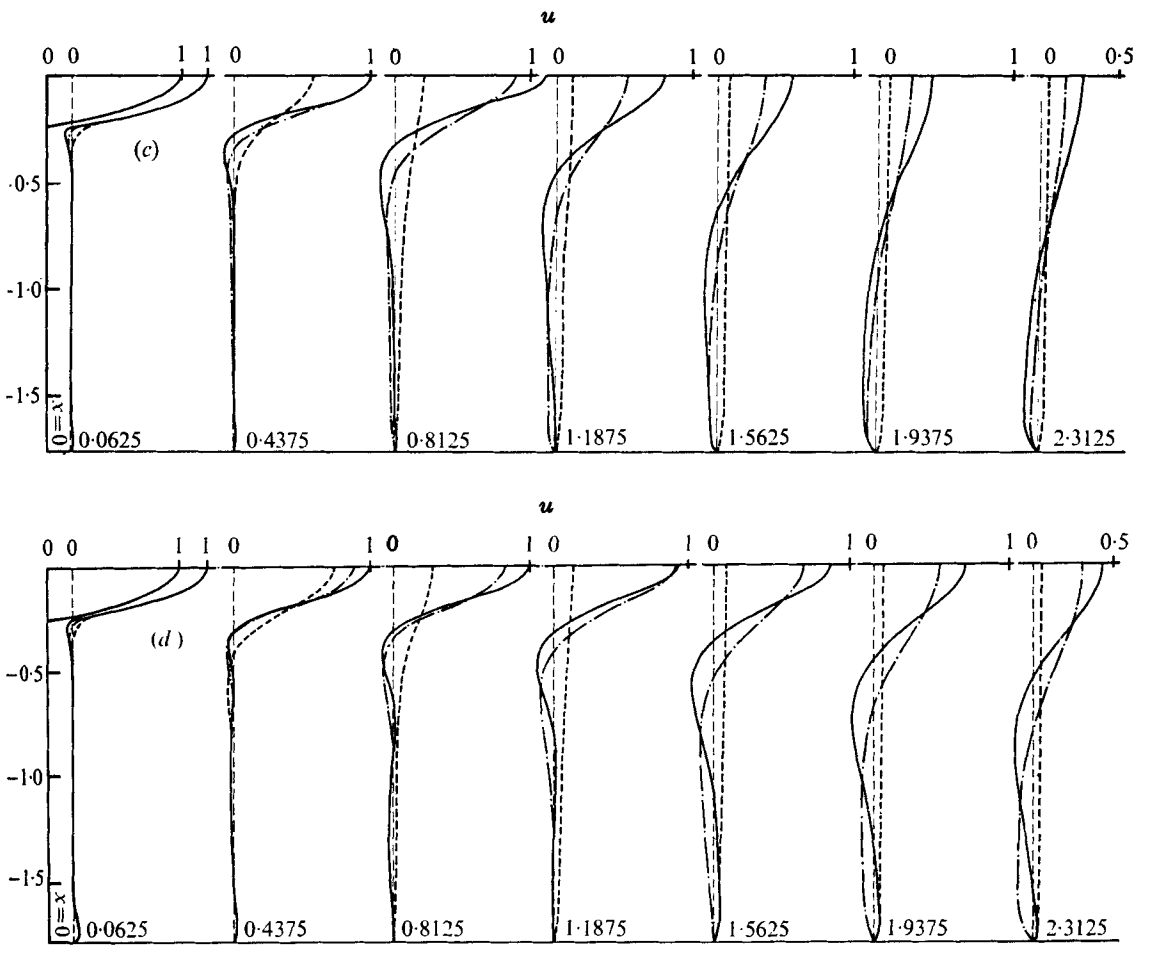

FIGURE 2. Horizontal velocity u; $R = 100$. ——, $F^{-2} = 64$; — · —, $F^{-2} = 32$; – – –, $F^{-2} = 0$. (*a*) $t = 0{\cdot}50$. (*b*) $t = 0{\cdot}75$. (*c*) $t = 1{\cdot}0$. (*d*) $t = 1{\cdot}50$.

highly unsteady in the case $R = 100$, $F^{-2} = 64$

$$(\max |\partial u/\partial t| = 0{\cdot}46, \quad \max |\partial v/\partial t| = 0{\cdot}59 \quad \text{and} \quad \max |\partial\theta/\partial t| = 0{\cdot}035)$$

and regions of reverse flow are continuously developing; even in the case $R = 100$, $F^{-2} = 0$ the flow is not steady at $t = 1{\cdot}50$.

In the case $R = 10$, $F^{-2} = 64$, an eddy appears near the entrance at $t \approx 0{\cdot}30$. However, this eddy is highly diffused and completely disappears as time goes on; moreover, no other eddy is created. The streamlines at $t = 0{\cdot}75$ and $t = 1{\cdot}50$ are shown in figures 4(*d*) and (*e*). At the latter time the flow is unsteady but the time derivatives are small ($\max |\partial u/\partial t| = 0{\cdot}057$, $\max |\partial v/\partial t| = 0{\cdot}048$ and $\max |\partial\theta/\partial t| = 0{\cdot}011$). The case $R = 10$, $F^{-2} = 0$ at $t = 1{\cdot}50$ (steady flow) is illustrated in figure 4(*f*).

It is apparent that in the case $R = 100$ the jet is constricted at some sections by the presence of eddies, so that the fluid is accelerated at these sections and

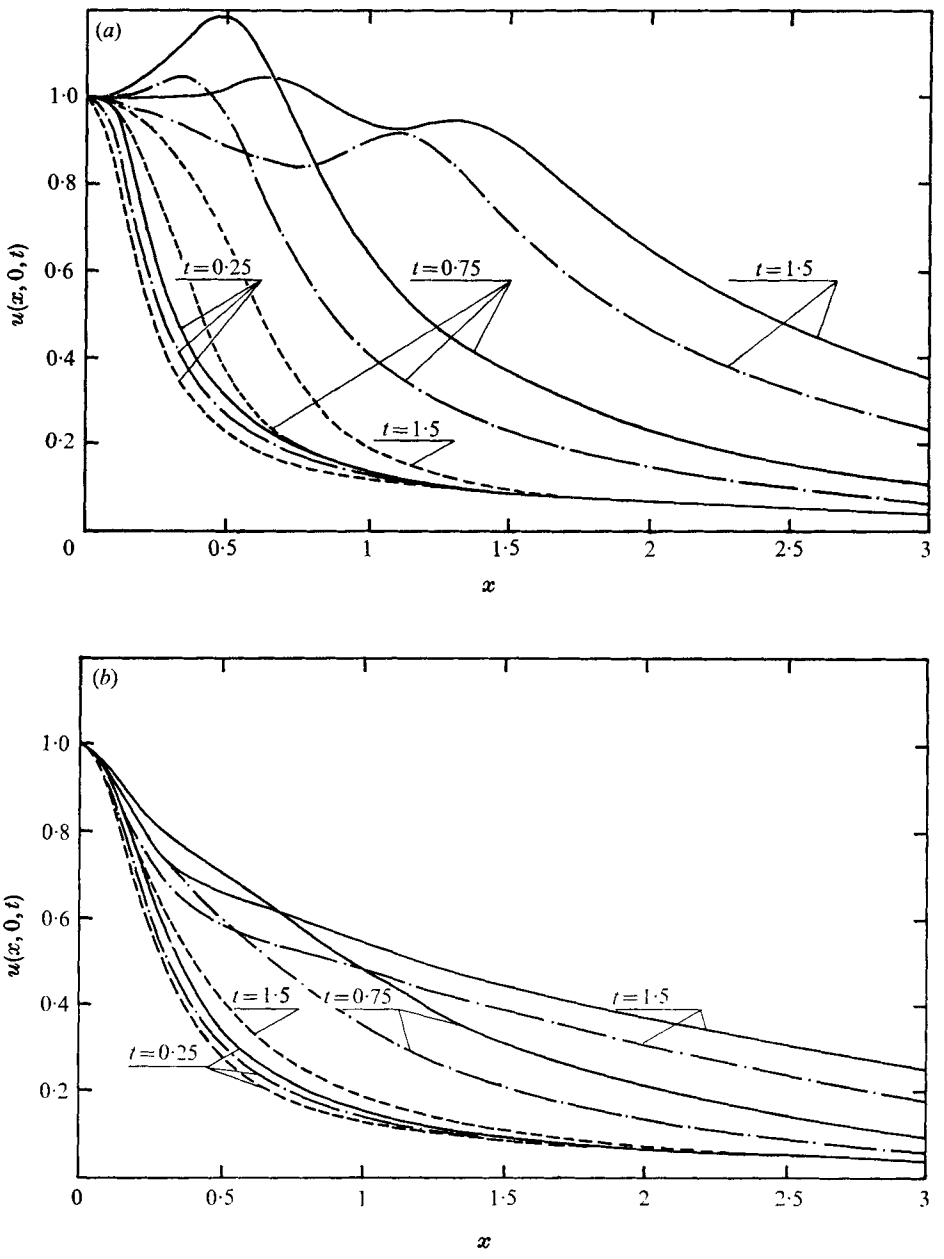

FIGURE 3. Velocity on the axis of symmetry. (*a*) $R = 100$. (*b*) $R = 10$. Curves as in figure 2.

the magnitude of the velocity on the axis can exceed its value at the entry; the oscillatory nature of certain curves in figure 3(*a*) reflects these constriction effects.

Maxworthy's experiments exhibit a 'slug' region or, more precisely, the progression of the injected fluid as a slender tongue of constant-density fluid

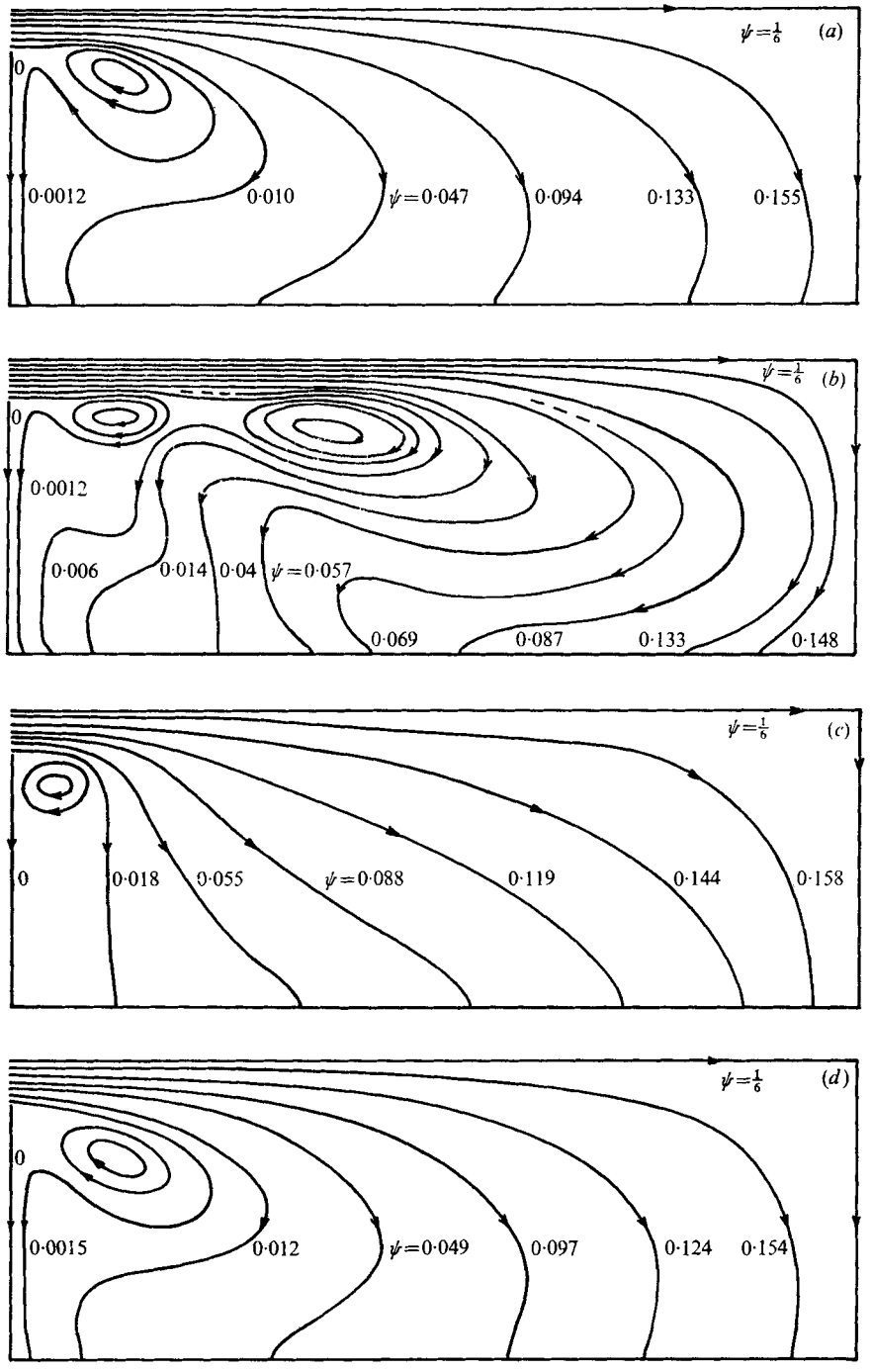

FIGURES 4(*a–d*). For legend see page 60.

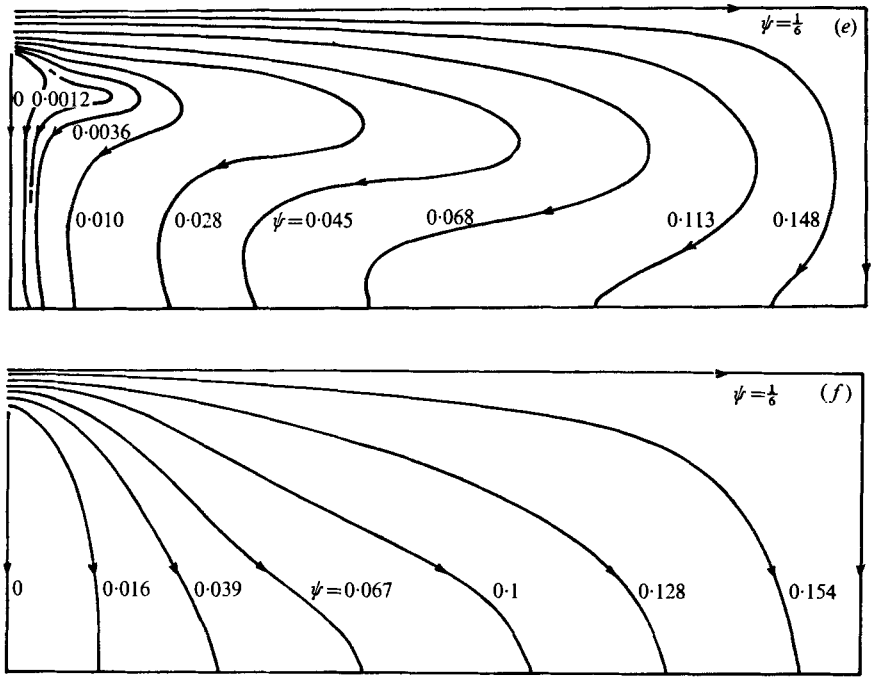

FIGURE 4. Streamlines.

	(a)	(b)	(c)	(d)	(e)	(f)
R	100	100	100	10	10	10
F^{-2}	64	64	0	64	64	0
t	0·75	1·50	1·50	0·75	1·50	1·50

with practically no diffusion into the surrounding fluid; the absence of diffusion was due to the fact that the experiments were performed with salt water. The present numerical results show a similar behaviour but it is less marked essentially because of the larger effect of thermal diffusion. Figure 5 shows some profiles of perturbation temperature θ, which is related to the perturbation density τ by $\tau = (\rho_2 - \rho_1)\theta/\rho_0$. The region with constant temperature $T = T_0$ (i.e. constant density $\rho = \rho_0$), which characterizes the 'slug', is delimited by dotted lines (points S at $t = 0{\cdot}75$ and S' at $t = 1{\cdot}50$).

Let us compare the temperature profiles at the two times $t = 0{\cdot}75$ and $t = 1{\cdot}50$. First of all we notice the heating near the axis $y = 0$, showing the progression of the 'slug' (up to $x = 1{\cdot}20$ approximately). Moreover, regions with increasing or decreasing temperature appear according to the general direction of the vertical flow, i.e. according as hot fluid is descending from upper layers or cold fluid is rising from lower layers.

The condition imposed on v at the horizontal boundary induces negative vertical velocities in the field; hence there is local heating yielding a tendency towards vertical uniformity of the temperature (outside boundary layers which survive owing to the boundary condition imposed on the temperature). For the times considered here ($t \leqslant 1{\cdot}50$) the phenomenon remains limited; however, if

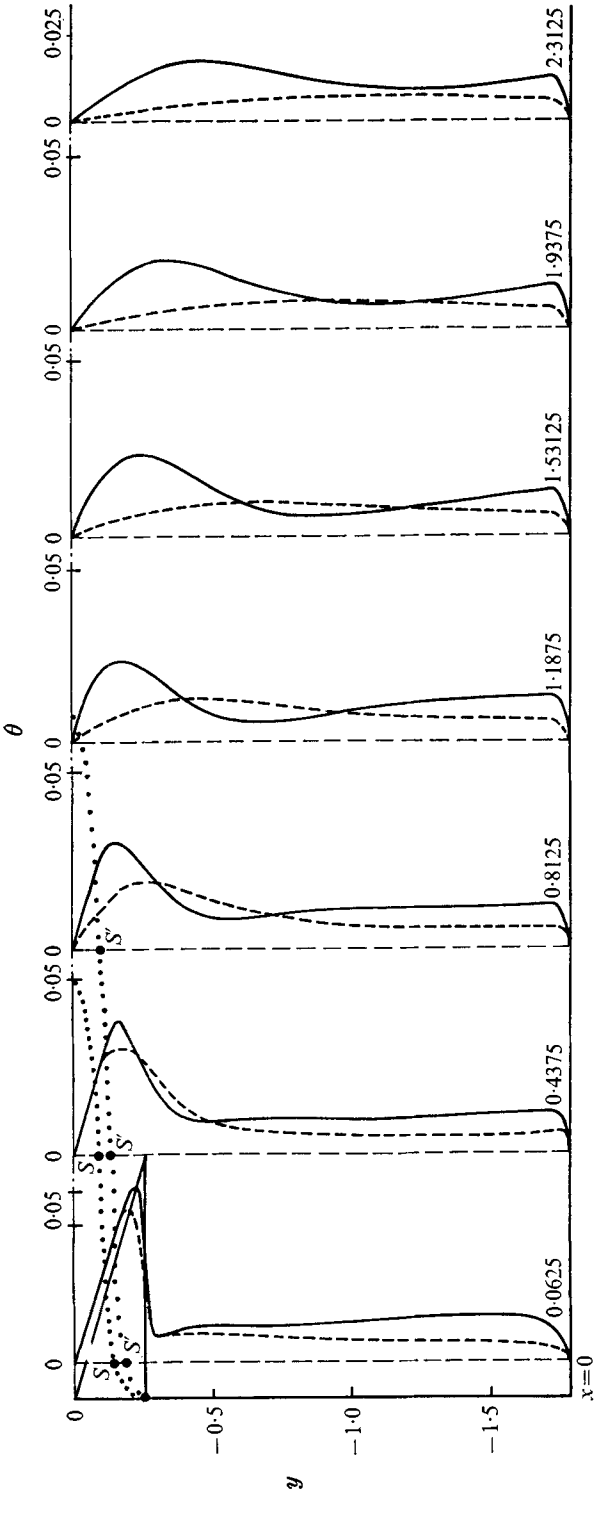

FIGURE 5. Temperature perturbation θ; $R = 100$, $F^{-2} = 64$. – – –, $t = 0{\cdot}75$; —, $t = 1{\cdot}50$.

the computations were continued to larger times, it might be desirable to minimize this effect by, for example, increasing the size of the tank.

The author is indebted to Prof. T. Maxworthy for suggesting the problem. This work has been partially supported by the National Science Foundation and the Office of Naval Research through grants to the University of Michigan for research on stratified flows. The author would like to express his thanks to Prof. C.-S. Yih for his hospitality and many helpful comments.

Appendix. Finite-difference equations

Let us introduce the first difference operators

$$(\delta_x^+ f)_{l,m} = (f_{l+1,m} - f_{l,m})/h,$$
$$(\delta_x^- f)_{l,m} = (f_{l,m} - f_{l-1,m})/h,$$
$$(\delta_x^0 f)_{l,m} = (f_{l+1,m} - f_{l-1,m})/(2h),$$
$$(\delta_x' f)_{l,m} = (-f_{l+2,m} + 8f_{l+1,m} - 8f_{l-1,m} + f_{l-2,m})/(12h),$$

and analogous operators δ_y^+, δ_y^-, δ_y^0 and δ_y' for the y differences; the discretized Laplacian operator is $\nabla_h^2 = \delta_x^+ \delta_x^- + \delta_y^+ \delta_y^-$. In the above expressions, h is the grid size and l and m may or may not be integers (e.g. $l = i, i+\frac{1}{2}, \ldots, m = j, j+\frac{1}{2}, \ldots$; see figure 6).

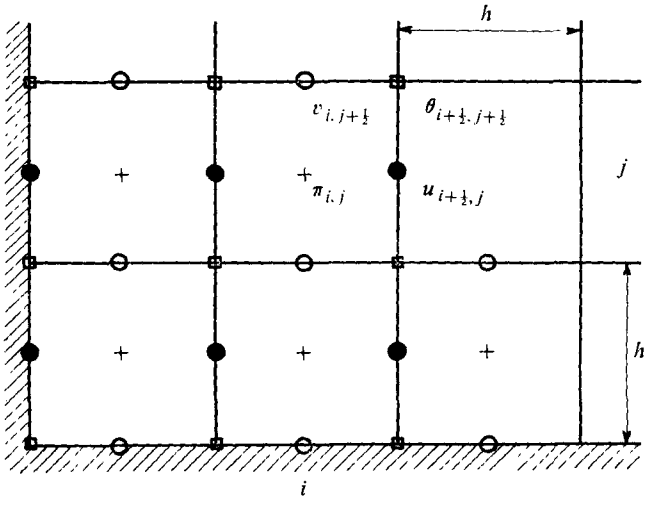

FIGURE 6. Discretization of x, y plane.

The finite-difference equations (4.1) have the following form (k is the time step):

$$\mathscr{L}_u \equiv k^{-1}(u^{n+1} - u^n)_{i+\frac{1}{2},j} + \tfrac{1}{2}[(u\delta_x^0 u)^{n+1} + (u\delta_x^0 u)^n]_{i+\frac{1}{2},j}$$
$$+ \tfrac{1}{2}[(\hat{v}\delta_y^0 u)^{n+1} + (\hat{v}\delta_y^0 u)^n]_{i+\frac{1}{2},j} + (\delta_x^+ \pi)_{i,j}^{n+\frac{1}{2}}$$
$$- (2R)^{-1}\nabla_h^2 (u^{n+1} + u^n)_{i+\frac{1}{2},j} = 0,$$

$$\mathscr{L}_v \equiv k^{-1}(v^{n+1} - v^n)_{i,j+\frac{1}{2}} + \tfrac{1}{2}[(\hat{u}\delta_x^0 v)^{n+1} + (\hat{u}\delta_x^0 v)^n]_{i,j+\frac{1}{2}}$$
$$+ \tfrac{1}{2}[(v\delta_y^0 v)^{n+1} + (v\delta_y^0 v)^n]_{i,j+\frac{1}{2}} + (\delta_y^+ \pi)_{i,j}^{n+\frac{1}{2}}$$
$$- (2R)^{-1}\nabla_h^2 (v^{n+1} + v^n)_{i,j+\frac{1}{2}} - \tfrac{1}{2}\eta F^{-2}(\bar{\theta}^{n+1} + \bar{\theta}^n)_{i,j+\frac{1}{2}} = 0,$$

$$\mathscr{L}_\theta \equiv k^{-1}(\theta^{n+1}-\theta^n)_{i+\frac{1}{2},j+\frac{1}{2}} + \tfrac{1}{2}[(\bar{u}\delta'_x\theta)^{n+1} + (\bar{u}\delta'_x\theta)^n]_{i+\frac{1}{2},j+\frac{1}{2}}$$
$$+ \tfrac{1}{2}[(\bar{v}\delta'_y\theta)^{n+1} + (\bar{v}\delta'_y\theta)^n]_{i+\frac{1}{2},j+\frac{1}{2}} + (2\eta)^{-1}(\bar{v}^{n+1}+\bar{v}^n)_{i+\frac{1}{2},j+\frac{1}{2}}$$
$$- (2RP)^{-1}\nabla_h^2(\theta^{n+1}+\theta^n)_{i+\frac{1}{2},j+\frac{1}{2}} = 0,$$
$$\mathscr{D} \equiv (\delta_x^- u)^{n+1}_{i+\frac{1}{2},j} + (\delta_y^- v)^{n+1}_{i,j+\frac{1}{2}} = 0,$$

where

$$\bar{u}_{i+\frac{1}{2},j+\frac{1}{2}} = \tfrac{1}{2}(u_{i+\frac{1}{2},j+1} + u_{i+\frac{1}{2},j}), \quad \bar{v}_{i+\frac{1}{2},j+\frac{1}{2}} = \tfrac{1}{2}(v_{i+1,j+\frac{1}{2}} + v_{i,j+\frac{1}{2}}),$$
$$\bar{\theta}_{i,j+\frac{1}{2}} = \tfrac{1}{2}(\theta_{i+\frac{1}{2},j+\frac{1}{2}} + \theta_{i-\frac{1}{2},j+\frac{1}{2}}), \quad \hat{u}_{i,j+\frac{1}{2}} = \tfrac{1}{2}(\bar{u}_{i+\frac{1}{2},j+\frac{1}{2}} + \bar{u}_{i-\frac{1}{2},j+\frac{1}{2}}),$$
$$\hat{v}_{i+\frac{1}{2},j} = \tfrac{1}{2}(\bar{v}_{i+\frac{1}{2},j+\frac{1}{2}} + \bar{v}_{i+\frac{1}{2},j-\frac{1}{2}}).$$

REFERENCES

Begis, D. 1972 Thèse de 3ème Cycle, Analyse Numérique, Université Paris VI.

Beavers, G. S. & Wilson, T. A. 1970 *J. Fluid Mech.* **44**, 97–112.

Childress, S. & Peyret, R. 1976 To be published in *J. Méc.*

Chorin, A. J. 1968 *Math. Comp.* **22**, 745–762.

Fortin, M. 1972 Thèse de doctorat d'Etat, Université Paris VI.

Fromm, J. E. 1967 *Fluid Dyn. Trans.* **3**, 169–191.

Gebhart, B. 1973 *Ann. Rev. Fluid Mech.* **5**, 213–246.

Graebel, W. P. 1969 *Quart. J. Mech. Appl. Math.* **22**, 39–54.

Grant, A. J. 1974 *J. Fluid Mech.* **66**, 707–724.

Harlow, F. H. & Welch, J. E. 1965 *Phys. Fluids*, **8**, 2182–2189.

List, E. J. 1971 *J. Fluid Mech.* **45**, 561–574.

Martin, S. & Long, R. R. 1968 *J. Fluid Mech.* **31**, 669–688.

Maxworthy, T. 1972 *Int. Symp. Stratified Flows, Novosibirsk.*

Pao, Y. H. 1968 *J. Fluid Mech.* **34**, 795–808.

Peyret, R. 1974 *C.R. Acad. Sci. Paris*, A **278**, 1569–1572.

Tenner, A. R. & Gebhart, B. 1971 *Int. J. Heat Mass Transfer*, **14**, 2051–2062.

Trent, D. S. & Welty, J. R. 1973 *Computers & Fluids*, **1**, 331–357.

Turner, J. S. 1973 *Buoyancy Effects in Fluids.* Cambridge University Press.

Wessel, W. R. 1969 *Phys. Fluids Suppl.* **12**, II 171–176.

Young, J. A. & Hirt, C. W. 1972 *J. Fluid Mech.* **56**, 265–276.